© 2017. Published by The Company of Biologists Ltd | Journal of Cell Science (2017) 130, 444-452 doi:10.1242/jcs.193771

RESEARCH ARTICLE

Vesicular PtdIns(3,4,5)P_3 and Rab7 are key effectors of sea urchin zygote nuclear membrane fusion

Marta G. Lete[1,2,3,*], Richard D. Byrne[4], Alicia Alonso[2], Dominic Poccia[5] and Banafshé Larijani[3,‡]

ABSTRACT

Regulation of nuclear envelope dynamics is an important example of the universal phenomena of membrane fusion. The signalling molecules involved in nuclear membrane fusion might also be conserved during the formation of both pronuclear and zygote nuclear envelopes in the fertilised egg. Here, we determine that class-I phosphoinositide 3-kinases (PI3Ks) are needed for *in vitro* nuclear envelope formation. We show that, *in vivo*, PtdIns(3,4,5)P_3 is transiently located in vesicles around the male pronucleus at the time of nuclear envelope formation, and around male and female pronuclei before membrane fusion. We illustrate that class-I PI3K activity is also necessary for fusion of the female and male pronuclear membranes. We demonstrate, using coincidence amplified Förster resonance energy transfer (FRET) monitored using fluorescence lifetime imaging microscopy (FLIM), a protein–lipid interaction of Rab7 GTPase and PtdIns(3,4,5)P_3 that occurs during pronuclear membrane fusion to create the zygote nuclear envelope. We present a working model, which includes several molecular steps in the pathways controlling fusion of nuclear envelope membranes.

KEY WORDS: Phosphoinositides, Src kinase, Zygote formation, Nuclear envelope, Membrane fusion, Rab GTPases, Phosphoinositide 3-kinase, FRET–FLIM

INTRODUCTION

The mechanisms by which nuclear envelopes are formed are not completely understood. It is generally agreed that, whether during mitosis, or during formation of the male pronuclear envelope around the sperm nucleus after fertilisation, the bulk of the nuclear envelope is derived from endoplasmic reticulum (ER) membranes that undergo fusion to enclose the chromatin (Burke and Ellenberg, 2002; Poccia and Larijani, 2009; Prunuske and Ullman, 2006). Fusion of complete male and female pronuclear envelopes to create the zygote nuclear envelope also occurs in many organisms (Byrne et al., 2014; Collas and Poccia, 1996b). Similarly, but less commonly, complete nuclear envelopes can form around individual chromosomes creating karyomeres, whose envelopes can fuse together to create complete nuclear envelopes around the full chromosome set (Domart et al., 2012).

On the basis of experiments on the *in vitro* and *in vivo* formation of the male pronuclear envelope, as well as *in vivo* data on zygote nuclear envelope formation and karyomere fusion, we have previously presented a common mechanistic model in which fusion is controlled upstream by a Src-family kinase (SFK1) that activates a phosphatidylinositide-specific phospholipase C (PLCγ) that catalyses the hydrolysis of PtdIns(4,5)P_2, resulting in the production of a fusogenic lipid, diacylglycerol (DAG) (Byrne et al., 2012, 2007, 2009a, 2014; Poccia and Larijani, 2009). The *in vitro* assays have been well documented over many years in several of our publications (Collas and Poccia, 1996a, 1998; Dumas et al., 2010), and the necessary controls, such as time-resolved Förster resonance energy transfer (FRET) analyses of nuclear envelope membrane fusion and electron micrographs, showing complete formation of the male pronucleus upon the GTP hydrolysis have been demonstrated.

These events are associated in the sea urchin with a subset of membrane vesicles (MV1) that had been isolated from egg cytoplasm that is highly enriched in SFK1, PLCγ and phosphorylated forms of phosphatidylinositol (Byrne et al., 2007, 2009b; Collas and Poccia, 1996a). Fusion with MV2 vesicles, which contain an ER marker, depends on and is initiated by the MV1 vesicles in male pronuclei (Collas and Poccia, 1996a; Dumas et al., 2010). Fusion requires GTP hydrolysis, but the GTPases responsible have not been identified. Male pronuclear envelope formation has also been shown to require phosphoinositide 3-kinase (PI3K) activity on the basis of inhibition by the relatively non-specific inhibitors wortmannin and LY29400 (Larijani et al., 2001). Connections with these potential upstream events remain to be elucidated.

Fusion in many membranous compartments of the cell has been linked to Rab GTPases (Stenmark, 2009). Members of the Rab family, often in conjunction with partner phosphoinositides, are fairly specific for different compartments, thus serving as identity markers. Rab proteins act as molecular switches as they swap between their GTP- and GDP-bound forms. Rabs generally participate in membrane trafficking and other events, and assist in the recruitment of various effector molecules. In fusion reactions, they can recruit tethering factors that specifically bind together the membranes to be fused. RAB escorts present Rabs to geranylgeranyl transferases for prenylation that permits their membrane recruitment from cytosol.

SFKs are recruited from the cytosol to the cytosolic face of membranes through palmitoylation (Sato et al., 2009). Changes in palmitoyl state can result in alternative localisations. Src is found in a large pool in late endosomes and/or lysosomes. Src that lacks palmitoyl groups but that has been myristoylated can exchange between plasma membrane and late endosomes and/or lysosomes.

[1]Cell Biophysics Laboratory, Ikerbasque Basque Foundation for Science, Research Centre for Experimental Marine Biology and Biotechnology (PiE) and Biofísika Instituto (UPV/EHU, CSIC), University of the Basque Country, Areatza Hiribidea, 47, 48620 Plentzia, Spain. [2]Biofísika Instituto (UPV/EHU, CSIC) and Departamento de Bioquímica, University of the Basque Country, Barrio Sarriena s/n, Leioa 48940, Spain. [3]Cell Biophysics Laboratory, Research Centre for Experimental Marine Biology and Biotechnology (PiE), Biofisika Instituto (UPV/EHU,CSIC) and, University of the Basque Country, Leioa 48940, Spain. [4]The Francis Crick Institute, Mill Hill Laboratory, The Ridgeway, London NW7 1AA, UK. [5]Department of Biology, Amherst College, Amherst, MA 01002, USA.
*Present address: Department of Molecular and Cellular Medicine, College of Medicine, Texas A&M Health Sciences Center, College Station, TX 77843-1114, USA.

‡Author for correspondence (banafshe.larijani@ikerbasque.org)

B.L., 0000-0003-4735-1169

Received 13 June 2016; Accepted 14 November 2016

Journal of Cell Science (2017) 130, 444-452 doi:10.1242/jcs.193771

It is unknown from which compartment SFK1-enriched MV1 vesicles arise.

Rab7 (of which there are two isoforms in mammals, Rab7a and Rab7b) is a monomeric GTPase that has been linked to SFK activity. The endocytic pathway is important for sorting proteins to be degraded in lysosomes or recycled to other membranous compartments in the cell. Late endosomes and/or lysosomes are associated with Rab7, which in conjunction with the ESCRT pathway, are needed for correct placement of Src within these organelles (Tu et al., 2011). ESCRT-III complexes have been implicated in the sealing of nuclear envelopes at a post-mitotic stage (Olmos et al., 2015; Vietri et al., 2015). Rab7 activity can be modified through interaction with PTEN, a phosphatase that prevents Rab7 from being recruited to late endosomes by GDP dissociation inhibitor protein (Shinde and Maddika, 2016). Coincidence detection of Rab7 and PtdIns(3)*P* by the ER protein protrudin promotes the formation of contact sites with late endosomes (Raiborg et al., 2015).

Both PtdIns(3)*P* and PtdIns(3,4,5)P_3 are much more abundant in MV1 than in MV2. Interestingly, Jethwa et al. (2015) have recently shown that PtdIns(3,4,5)P_3 is enriched in both the nuclear envelope and early endosomal membranes.

Because nuclear envelope formation in sea urchin depends on PI3Ks of unknown class and on GTP hydrolysis by unidentified GTPases, we tested whether class-I kinases are required for nuclear envelope formation and examined where PtdIns(3,4,5)P_3 is located and whether Rab7 interacts with PtdIns(3,4,5)P_3.

Here, using the specific class-I PI3K inhibitors PIK-75 and BYL719, we report that class-I PI3Ks are needed for *in vitro* nuclear envelope formation. Using a GRP-1 plextrin homology (PH) domain specific for PtdIns(3,4,5)P_3 detection, we show that this phospholipid is transiently located in vesicles around the male pronucleus at the time of nuclear envelope formation, and around male and female pronuclei *in vivo* before membrane fusion. Pronuclear envelope fusion is also blocked by specific class-1 PI3K inhibitors (PIK-75 and BYL719). Finally, using time-resolved coincidence amplified-FRET monitored by performing fluorescence lifetime imaging microscopy (FLIM), we show, for the first time, a protein–lipid interaction of Rab7 and PtdIns(3,4,5)P_3. We discuss models to account for the roles of Rab7 and PtdIns (3,4,5)P_3 in nuclear envelope formation and fusion.

RESULTS

To determine the upstream effectors of the fusion machinery [PLC, SFK1 PtdIns(4,5)P_2 and DAG] that are implicated in nuclear envelope formation (Byrne et al., 2007, 2009a, 2014; Poccia and Larijani, 2009), we set out to test the involvement of the class-I PI3Ks and their product PtdIns(3,4,5)P_3. These experiments were performed initially in cell-free assays and afterwards *in situ* using intact fertilised sea urchin (*Paracentrotus lividus*) eggs.

Class-I PI3Ks are required for nuclear envelope formation *in vitro*

Using the cell-free assay, we tested the class-I-PI3K-specific inhibitors PIK-75 and BYL719, which block the kinase activity through competitive inhibition at the substrate-binding site and at the ATP-binding sites, respectively. The reaction was terminated after 1 h of incubation with the ATP-generating system; here membrane vesicles were bound to chromatin, but they did not fuse. Upon addition of GTP, the nuclear envelope formed a continuous membrane around the nuclei. The addition of the two PI3K-specific inhibitors resulted in the malformation of the nuclear membrane (Fig. S1A). As mentioned above, membrane fusion in these *in vitro* assays has been previously demonstrated by time-resolved FRET (Dumas et al., 2010). Therefore, the fluorescent assays were used here to quantify nuclear envelope formation. The assays were performed with and without inhibitor by scoring 100 nuclei for each condition. Upon addition of GTP, more than 70% of the nuclei had complete nuclear membranes. In all cases, 0.35 µl of DMSO was added after the first incubation as a vehicle control. Two different concentrations of LY 294002, a general PI3K inhibitor, were used as positive controls, and the PIK-75 inhibitor that is specific for class-I PI3Ks was added with the same DMSO volume as in the controls. After a 2-h incubation with GTP, the number of nuclei with a continuous nuclear envelope were scored. A significant decrease in nuclear envelope formation was observed with PIK-75 and BYL19 (Fig. 1).

These results indicate that PtdIns(3,4,5)P_3 formation was a requirement for nuclear envelope formation. To determine localisation of PtdIns(3,4,5)P_3, we used the PH domain of general receptor for phosphoinositides 1-associated scaffold protein (Grp1), which recognises PtdIns(3,4,5)P_3 selectively (Ferguson et al., 2000; Klarlund et al., 2000). The Grp1 PH domain was co-purified with a GST tag, and its *in vitro* affinity was tested, as described previously (Jethwa et al., 2015). PtdIns(3,4,5)P_3 was added *in vitro* to the cell-free assay. In these experiments, the reaction was terminated at different stages, firstly after the ATP addition, secondly 30 min after the GTP addition and, thirdly, two hours after GTP addition when the assembly was completed. Fig. S1B shows the punctate localisation of PtdIns(3,4,5)P_3 both during binding of the membrane vesicles and their fusion. The addition of PIK-75 resulted in a reduction of the fluorescence intensity of the punctate localisation of PtdIns(3,4,5)P_3. The inhibition did not reduce the number of punctate regions but it did reduce the fluorescence intensity.

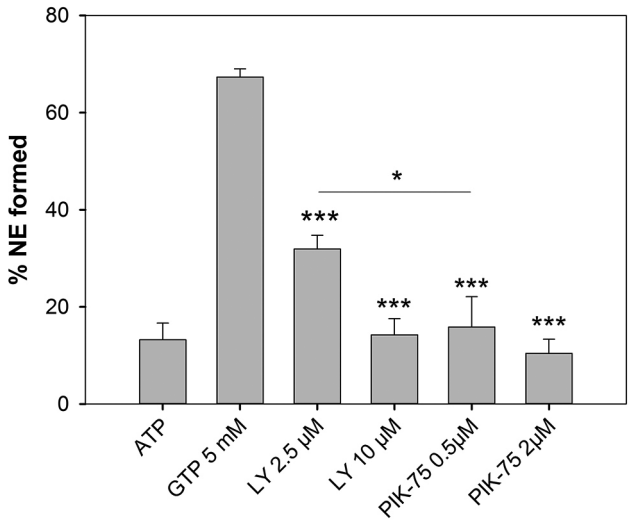

Fig. 1. Class-I PI3Ks are required for nuclear envelope formation *in vitro*. The percentage of nuclear envelopes (NE) formed (i.e. nuclei fully enclosed by membranes) under different conditions – the presence of ATP, a positive control with 5 mM GTP, the general PI3K inhibitor LY 294002 and class-I-specific PI3K inhibitor (PIK-75) (used at the indicated concentrations). Nuclear envelope formation was significantly blocked with both inhibitors, but more efficiently by the class-I-specific PI3K inhibitor. Three independent sets of experiments were performed. In each experiment, at least 100 nuclei were scored. Error bars indicate s.d. and the means are shown. *** denotes a very significant reduction (*t*-test $P<0.001$) of nuclear envelope formed in the inhibitor-treated samples compared with in the GTP-positive sample. *$P<0.05$.

Journal of Cell Science (2017) 130, 444-452 doi:10.1242/jcs.193771

These results demonstrate the involvement of both class-I PI3Ks and PtdIns(3,4,5)P_3 in the *in vitro* formation of the nuclear envelope.

PtdIns(3,4,5)P_3 is localised at the male and female pronuclei *in situ*

Because PtdIns(3,4,5)P_3 was necessary for the *in vitro* formation of the nuclear membrane, we used the same probe, GST–Grp1-PH, to further explore its role in the various membrane fusion events that take place in the fertilised sea urchin egg. We specifically focussed on the female and the male pronuclear fusion. Fig. 2 shows immunofluorescence experiments that were performed using this probe. PtdIns(3,4,5)P_3 membrane vesicles were localised at the egg cortex during the first stages of fertilisation, whereas at the later stages (7 min), a recruitment of the PtdIns(3,4,5)P_3 vesicles at the male pronucleus and, at 10–20 min, at the female pronucleus was observed. At 30 min, following the fusion of the male and female pronuclei, the PtdIns(3,4,5)P_3 vesicles once again showed a cortical localisation.

Inhibition of class-I PI3Ks abrogates continued fusion of male and female pronuclei

To investigate the role of class-I PI3Ks in pronuclear fusion, we used, as in the *in vitro* experiments, PIK-75. PIK-75 was added to *P. lividus* eggs 4 min after fertilisation. Fertilisation was terminated by fixing the eggs at different time points before the first cell division. Vehicle controls were performed by adding the same volume of DMSO alone. The effect of the inhibitor *in situ* was characterised by measuring the distance between the male pronucleus and the female pronucleus when treated with 1 µM PIK-75 or without inhibitor at different times post fertilisation (Fig. 3). Fusion was scored as the merging of the male and female chromatin DNA stains. At 15 min, when there is an accumulation of PtdIns(3,4,5)P_3 vesicles, the male and female pronuclei had not yet fused. It was only two minutes later, at 17 min post fertilisation, that the male pronucleus and the female pronucleus were in close contact and mostly fused. However, in eggs that had been treated with 1 µM PIK-75, a substantially lower percentage had fused although most were in proximity. The quantification demonstrates that the inhibition of class-I PI3Ks prevented the continued fusion of the male and female pronuclei but not the accumulation of PtdIns(3,4,5)P_3 vesicles, hence demonstrating the requirement of class-I PI3Ks for this fusion event.

PtdIns(3,4,5)P_3 and Rab7 vesicles colocalise in the pronuclear region

We postulated that, as in the maturation of late endosomes in mammalian cells, the small GTPase Rab7 would be in the same compartment as SFKs (Stenmark, 2009) and that PtdIns(3,4,5)P_3 would be involved in the recruitment of Rab7, where it might lead to the recruitment of SFK1 to activate PLCγ (Byrne et al., 2012). To test this hypothesis, we performed a series of immunofluorescence experiments to determine the localisation of PI3K and its substrate and product PtdIns(4,5)P_2 and PtdIns(3,4,5)P_3, respectively (Fig. 4A–B). The immunofluorescence experiments also showed the localisation of Rab7 and PtdIns(3,4,5)P_3 (Fig. 4C), and of SFK and Rab7 (Fig. 4D). All colocalisations were quantified in whole eggs as well as in the regions of the pronuclei at the 7- and 15-min time points. The box and whisker plots show a significant colocalisation of PI3K and PtdIns(4,5)P_2 at 7 min in the pronuclear region. Rab7 and SFK1 colocalisation were significant in the whole egg at 7 min, whereas significant differences were not observed between 7 and 15 min. The most significant colocalisation was between Rab7 and PtdIns(3,4,5)P_3 at 15 min in the pronuclear region where PtdIns(3,4,5)P_3 vesicles were recruited (Fig. 2) for the fusion of the male and female pronuclei.

In addition to indicating that Rab7 and SFK1 might share the same vesicle in the MV1 population, these results illustrate for the

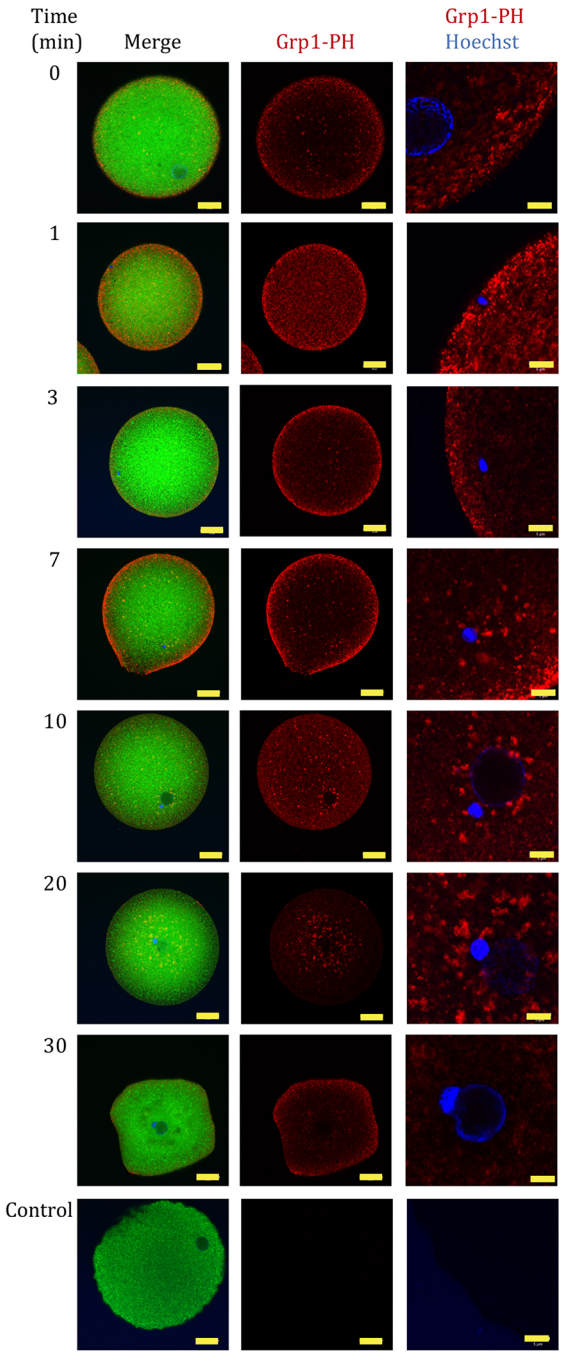

Fig. 2. PtdIns(3,4,5)P_3 is localised at the male and female pronuclei *in situ*. Nuclei were labelled with Hoechst 33342 (blue), membranes with $DiOC_6$ (green) and PtdIns(3,4,5)P_3 with the purified GST–Grp1-PH (Grp1-PH) probe tagged with a conjugated anti-GST antibody (red), and imaged by confocal microscopy. Fertilised *P. lividus* eggs were fixed at different times post fertilisation. PtdIns(3,4,5)P_3 vesicles were observed around the eggs upon fertilisation, mostly accumulating between 10 and 20 min, and close to the male and female pronuclei at fusion. The secondary antibody controls were performed by adding an anti-GST antibody alone. Scale bars: 20 µm (whole egg); 5 µm (zoom).

Journal of Cell Science (2017) 130, 444-452 doi:10.1242/jcs.193771

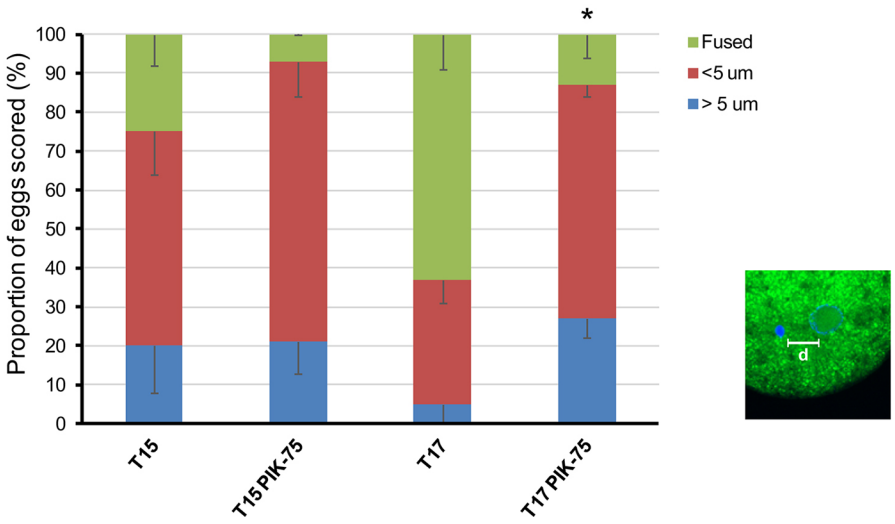

Fig. 3. Inhibition of class-I PI3Ks abrogates continuous fusion of male and female pronuclei. *P. lividus* eggs were fertilised, and 4 min after fertilisation treated with 1 µM PIK-75. Eggs were fixed at different times post fertilisation. Vehicle controls were performed by adding the same volume of DMSO as of the inhibitor. Male and female pronuclei were labelled with Hoechst 33342 (blue), and the distance between the male and female pronuclei was observed by confocal microscopy and analysed using ImageJ (see inset for example; d, distance). Each colour corresponds to the distance between the pronuclei of vehicle control eggs at the indicated times post fertilisation (T15, 15 min) or of inhibitor-treated eggs after the indicated time [PIK-75 (T15), 15 min in the presence of inhibitor]. For each condition, at least 25 eggs were scored. Error bars indicate s.e.m.

first time the localisation and quantified colocalisation of PtdIns(3,4,5)P_3 and Rab7 during zygote nuclear membrane fusion.

PtdIns(3,4,5)P_3 and Rab7 interact in vesicles around the forming zygote nuclear envelope

The quantified colocalisations between PtdIns(3,4,5)P_3 and Rab7 vesicles indicated that these effectors were within the same vicinity. To determine whether PtdIns(3,4,5)P_3 and Rab7 actually interacted during zygote nuclear membrane fusion, we exploited coincidence amplified time-resolved FRET (a-FRET) (Byrne et al., 2014). This method has been described in detail previously (Byrne et al., 2014; Veeriah et al., 2014). Briefly, Rab7 was labelled using a primary monoclonal antibody conjugated to an anti-chicken F(ab′)$_2$–Atto488 (the donor). The PtdIns(3,4,5)P_3 labelling was performed with GST–Grp1-PH, an antibody against GST that had been conjugated to a secondary anti-rabbit F(ab′)$_2$ that had been labelled with horseradish peroxidase (HRP) and Alexa-Fluor-594 (the acceptor). The main difference from previously published a-FRET methods was that here, for the first time, we exploited a-FRET to determine protein–lipid interactions instead of protein–protein interactions.

Fig. 5 shows box and whisker plots of the lifetime distributions of the donor alone, of the donor and acceptor, and of the donor in the presence of the ‘false acceptor’ control. All the lifetime measurements were acquired using an oil immersion 60.3× objective, a wide-field microscope and multiple frequency domain FLIM. In unfertilised eggs, the lifetime distributions did not significantly change (Fig. 5A). However, at 15 min post fertilisation, donor lifetime decreased significantly in the pronuclear region (Fig. 5B). The lifetime was recovered to the donor lifetime with the ‘false acceptor’ control (Rab7+HRP). The calculated FRET efficiencies between unfertilised and 15 min fertilisation were 0% and 10%, respectively.

These data indicate that Rab7 and PtdIns(3,4,5)P_3 were not just co-localised but were actually interacting during male and female pronuclear fusion. This interaction could explain the reason for the accumulation of PtdIns(3,4,5)P_3 vesicles at the 10-min time point (Fig. 2).

DISCUSSION

Recently, Byrne et al. (2012) have shown, using time-resolved FRET, the spatially restricted and direct molecular interaction of PLCγ and SFK1 during the formation of the male pronuclear envelope. They have shown that during GTP initiation of nuclear membrane precursor fusion, PLCγ is phosphorylated on residue Tyr783, which is dependent on SFK1 activity. Transient phosphorylation of Tyr783 was detected on the surface of the male pronuclei *in vivo* during formation of the nuclear envelope. Kinetic analysis led to a model in which vesicles enriched in SFK1, PLCγ and PtdIns(4,5)P_2 are bound to the nuclei under conditions in which SFK1 is inactive. GTP hydrolysis then removes the inhibition, allowing SFK1 to phosphorylate PLCγ, which hydrolyses the PtdIns(4,5)P_2 to locally produce fusogenic DAG, leading to membrane fusion and nuclear envelope formation. After initiation of fusion, SFK1 and PLCγ remain on the nuclear envelope but no longer directly interact.

Byrne et al. (2014) have shown more recently that a similar mechanism accounts for the fusion of the new male pronuclear envelope with the already formed female pronuclear envelope during the first embryonic cell cycle to create the zygote nuclear envelope. Once again, PLCγ and SFK1 were shown, using time-resolved FRET, to directly interact at the site of nuclear membrane fusion where PtdIns(4,5)P_2 levels are lower.

In karyomere fusion, alteration of DAG levels through microinjection of DAG-modifying enzymes that either deplete its precursor or convert it to phosphatidic acid slow or block karyomere nuclear envelope fusion. In addition, these treatments block or delay mitotic nuclear membrane reformation in both sea urchin and mammalian cells (Domart et al., 2012).

Taken together, these data suggest a conserved mechanism for nuclear envelope formation and membrane fusion. Despite the abundant evidence suggesting a new role for DAG and its upstream control by SFK1 and PLCγ in nuclear envelope fusion events, the nature of the small GTPase and PI3K requirements remain unclear, as does the mechanism for fusion propagation within the MV2 population, which creates the complete nuclear envelope. Recently, Jethwa et al. (2015) have shown that PtdIns(3,4,5)P_3 is enriched in both the nuclear envelope and early endosomal membranes. By using the selective inhibitor PIK-75, which binds to the p100α subunit (encoded by *PIK3CA*) of class-I PI3Ks, they showed that depletion of PtdIns(3,4,5)P_3 lowered activation of targeted PKB/Akt in the early endosomal and nuclear envelope compartments, suggesting that PtdIns(3,4,5)P_3 resides in endomembranes such as the early endosomes and the nuclear envelope.

On the basis of experiments shown here, we suggest that PtdIns(3,4,5)P_3 also has a role in recruiting the fusion machinery necessary for the formation of the zygote nuclear membrane that results from

Journal of Cell Science (2017) 130, 444-452 doi:10.1242/jcs.193771

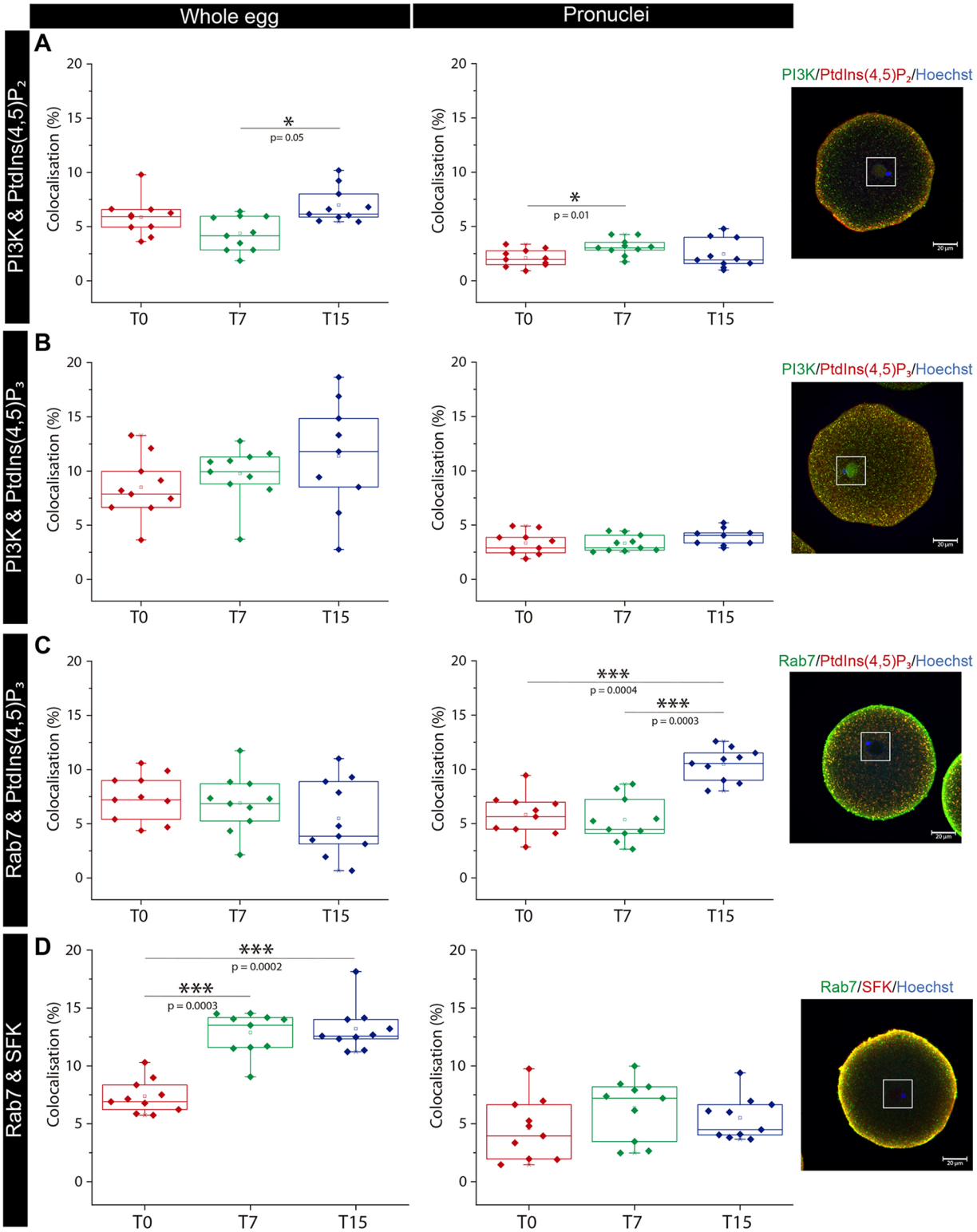

Fig. 4. Rab7 and SFK1 colocalise post fertilisation, and PtdIns(3,4,5)P_3 and Rab7 vesicles colocalise at the pronuclei region. Multiple eggs were analysed at three different stages – unfertilised (T0), and 7 and 15 min after fertilisation (T7 and T15, respectively). The colocalisation of proteins and phosphoinositides in each egg was quantified for the whole egg (left column), and for the region surrounding the pronuclei (right column). A representative confocal image of an egg at 15 min after fertilisation is next to each plot; the square corresponds to the region where colocalisation was measured separately from that in the rest of the cytoplasm. (A) Increase of colocalisation of PtdIns(4,5)P_2 and class-I PI3Ks after fertilisation around the male pronucleus. (B) Class-I PI3K colocalisation with their product PtdIns (3,4,5)P_3. (C) PtdIns(3,4,5)P_3 vesicles surrounding the pronuclei of fertilised eggs colocalised significantly more with Rab7 than in unfertilised eggs, suggesting a recruitment of the GTPase. (D) Post fertilisation, the colocalisation of Rab7 and SFK1 (SFK) in the egg cortex was significantly increased, which could lead to activation of SFK1. Images were quantified using Imaris image software, and data are expressed as box and whisker plots, where the line indicates the median, the square indicates the mean, the box indicates the 25–75th quartiles of the population, whiskers represent the minima and maxima values, and individual data points are shown as diamonds. For the statistical analysis, a non-parametric Mann–Whitney test was performed; *P≤0.05, ***P≤0.001. Hoechst, Hoechst 33342.

Journal of Cell Science

Journal of Cell Science (2017) 130, 444-452 doi:10.1242/jcs.193771

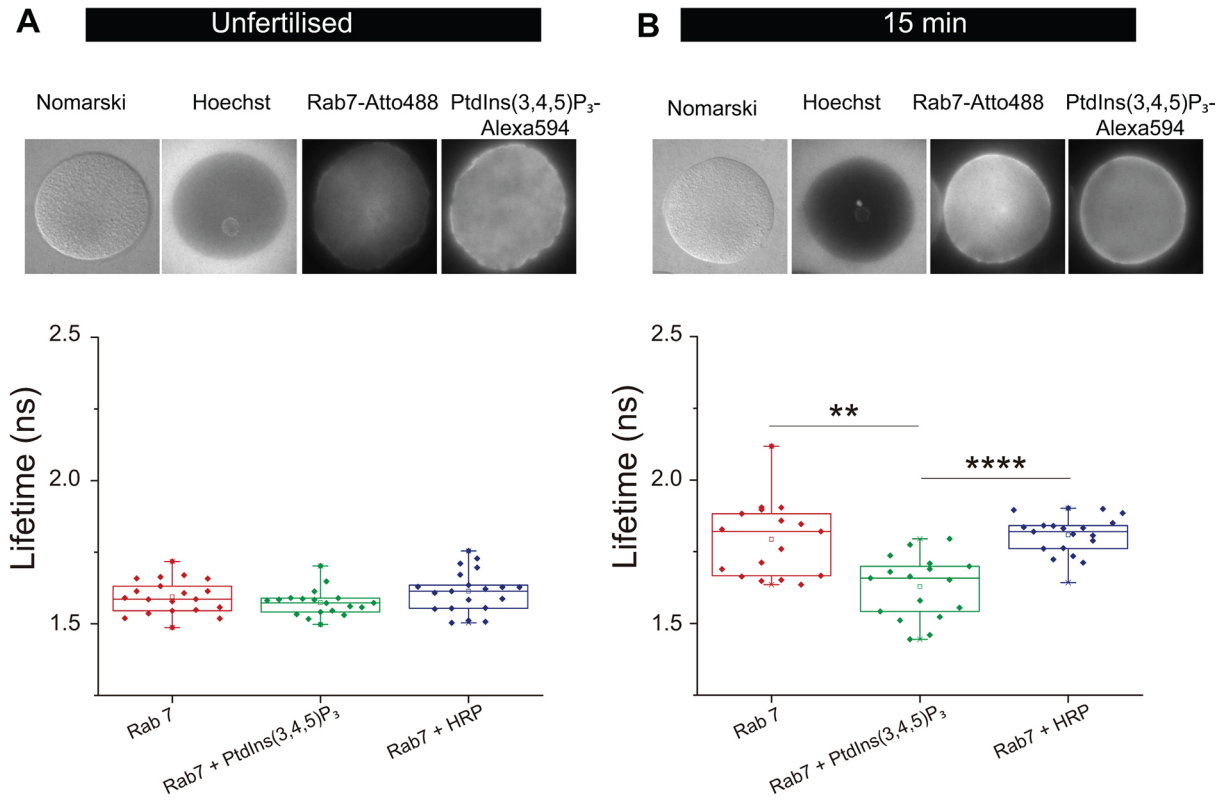

Fig. 5. PtdIns(3,4,5)P_3 and Rab7 vesicles interact around the new zygote. The *in situ* lipid–protein interactions were determined by using coincidence amplified-FRET detected by FLIM. Fixed sea urchin eggs were labelled with anti-Rab7 antibody conjugated to Atto-488 (donor), anti-Rab7 antibody conjugated to Atto-488 and PtdIns(3,4,5)P_3–HRP–Alexa-Fluor-594 (donor and acceptor), or to anti-Rab7 antibody conjugated to Atto-488 and HRP–Alexa-Fluor-594 (donor and false-acceptor–HRP control). The donor's lifetime was determined under these three conditions in (A) unfertilised eggs and (B) in eggs at 15 min post fertilisation. Nomarski and fluorescence intensity images of donor alone and donor+acceptor images are shown above the lifetime box and whisker plots. Lines indicate the medians, the squares indicate the mean, the boxes indicate the 25–75th quartiles of the population, whiskers represent the minima and maxima values, and individual data points are shown as diamonds. A significant decrease in the lifetime at 15 min illustrates the interaction of PtdIns(3,4,5)P_3 and Rab7 vesicles. The reversal of lifetime to donor lifetime alone with the HRP control indicates the specificity of the interaction determined using FRET. For each condition, 20 eggs were analysed. Every egg was divided into two regions of interest, first a region encompassing the cytoplasm and a second region surrounding the pronuclear region. A non-parametric Mann–Whitney test was used for the statistical analysis. $^{**}P \leq 0.01$ and $^{****}P \leq 0.0001$.

fusion of male and female pronuclei. It should be noted that, in this model, formation of PtdIns(3,4,5)P_3 is not transient as in the case of the mammalian plasma membrane. In sea urchin, vesicles stably enriched in PtdIns(3,4,5)P_3 and PtdIns(4,5)P_2 are recruited to the sites of fusion. The quantitative colocalisation experiments showed an enhancement of vesicles containing Rab7 and SFK1, suggesting a role for both of these effectors during the zygote nuclear envelope formation. The localisation of PtdIns(3,4,5)P_3-containing vesicles around the female pronucleus and the prevention of zygote nuclear envelopes by class-1 PI3K inhibitors indicate an important role for PtdIns(3,4,5)P_3 during the male and female pronuclei fusion. Furthermore, the spatiotemporal FRET results show a direct interaction of PtdIns(3,4,5)P_3 and Rab7 during zygote nuclear membrane formation. The *in situ* involvement of PtdIns(3,4,5)P_3 and Rab7 vesicles in a membrane fusion event is a new finding.

Colocalisation of SFK1 and Rab7 strongly suggests that they co-exist in MV1 vesicles along with PtdIns(3,4,5)P_3, PtdIns(4,5)P_2 and PLCγ. The function of the minor membrane fraction MV1 in initiation of fusion of male pronuclear membrane precursors (Dumas et al., 2010) suggests an analogous role in male and female pronuclear envelope fusion as well.

MV1 vesicles are located mostly in the egg cortex before fertilisation where they might aid cortical vesicle and/or plasma membrane fusion; they might also initiate fusion of male pronuclear envelope precursors of the MV2 class within a few minutes of fertilisation (Byrne et al., 2012; Dumas et al., 2010). Later MVIs are found to be associated with the male and female pronucleus envelopes as they fuse (Byrne et al., 2014; this paper). Thus, MV1 could represent a relatively stable assembly that comprises a regulated mobile nuclear envelope fusion platform.

A working model for control of pronuclear envelope fusion is shown in Fig. 6. MV1 components, comprising Rab7, SFK1 and PLCγ, are preassembled in a stable fusion platform in MV1 vesicles that are highly enriched in PtdIns(3,4,5)P_3 and PtdIns(4,5)P_2. The platform is inactive because SFK1 is inhibited by a putative C-terminal Src-kinase (Csk) protein, a non-receptor tyrosine kinase that phosphorylates an inhibitory tyrosine site in the N-terminal region of Src-family kinases.

MV1 vesicles contain mixed populations of PtdIns(3,4,5)P_3, PtdIns(4,5)P_2, SFK1, PLCγ and Rab7. Vesicles containing only some of these components stably associate with other vesicles that carry the missing phosphoinositides or proteins; these vesicles associate in close enough proximity to allow for the FRET interactions that have been reported (Byrne et al., 2014; this paper). The maintenance of fusogenic properties requires class-I PI3K activity, probably to keep the concentration of PtdIns(3,4,5)P_3 elevated in the face of potential 3-phosphatase activity.

Journal of Cell Science (2017) 130, 444-452 doi:10.1242/jcs.193771

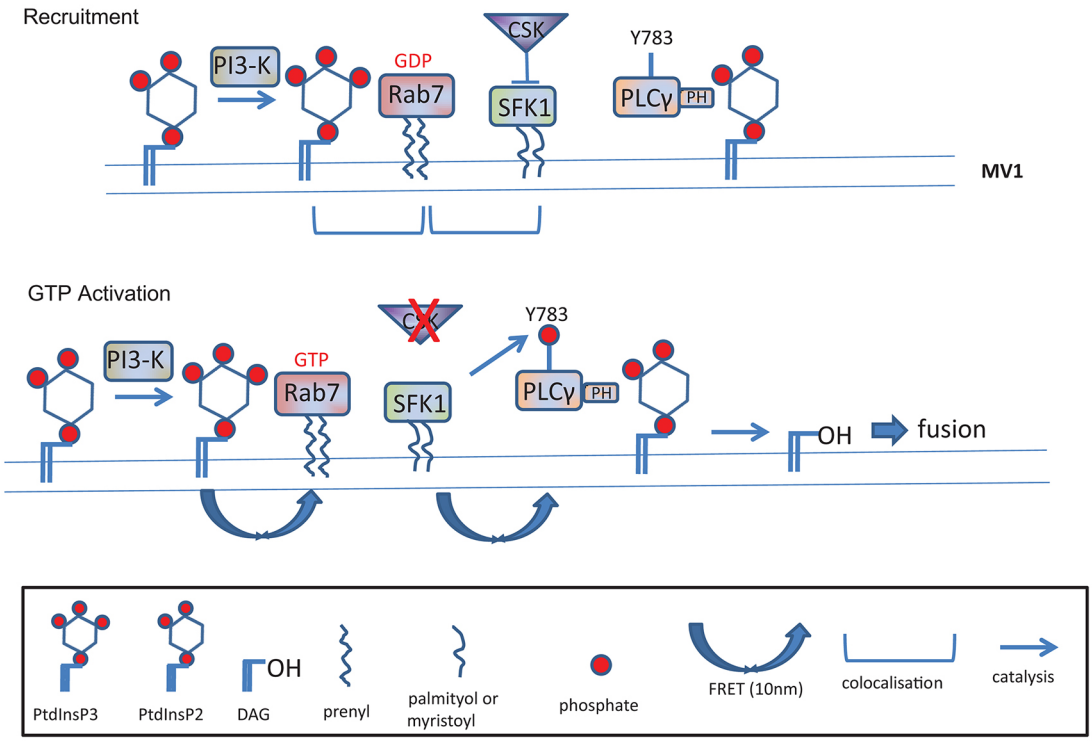

Fig. 6. Working model of the nuclear envelope fusion platform. Vesicles that are enriched in PtdIns(3,4,5)P_3 and PtdIns(4,5)P_2 assemble with inactive Rab7, SFK1 and PLCγ. PtdIns(3,4,5)P_3 is maintained by a class-I PI3K and is recognised by both Rab7 and PLCγ. Curved arrows indicate the FRET interactions demonstrated here; brackets indicate colocalisation. Initiation of membrane fusion by GTP activates Rab7 and removes the block to SFK1 activity, possibly caused by Csk inhibition. Phosphorylation of PLCγ by SFK1 on Tyr783 activates it, catalysing the hydrolysis of PtdIns(4,5)P_2 to the fusogenic lipid diacylglycerol. Other, as yet unidentified, proteins are likely to be recruited and assembled in the platform by Rab7.

GTP can locally initiate the fusion pathway. GTPase activity removes the block to SFK activity. It is not known how many steps occur between GTPase and SFK activation, or whether multiple GTPases are active. SFK1 phosphorylation of PLCγ then initiates local elevation of the fusogenic lipid DAG, which initiates fusion of the two pronuclear envelopes to form a zygote nuclear envelope.

The possibility of pre-assembling an inactive membrane fusion complex in vesicles transported to the site at which fusion will take place would offer a new addition to a repertoire of fusion mechanisms that are available in the cell. Involvement of Rab7 and the maintenance of PtdIns(3,4,5)P_3 represent additional upstream components to the machinery that is required for nuclear membrane fusion events.

MATERIALS AND METHODS

Materials

P. lividus sea urchins were purchased from Macrae and company, or collected from the coast of Armintza (Basque Country). 3′3-Dihexyloxacarbocyanine iodide ($DiOC_6$), Hoechst 33342, ProLong antifade reagent, and chemically competent *Escherichia coli* MAX efficiency DH5α, peroxidase suppressor and tyramide signal amplification (TSA) kit with Alexa-Fluor-594 tyramide were from Invitrogen Life Technologies. Anti-PI3K p85 antibody (# 86714; 1:100), anti-Rab7 antibody (# 50533; 1:100), donkey anti-mouse IgG conjugated to Alexa-Fluor-488 (# 150105; 1:200), goat anti-chicken IgY conjugated to Alexa-Fluor-647 (# 150171; 1:500), goat polyclonal antibody to GST conjugated with DyLight650 (# 117497; 1:500) and anti-GST antibody (# 9085; 1:500) were from Abcam. AffiniPure F (ab′) 2 IgG anti-mouse (# 715-006-150; 1:500) and peroxidase AffiniPure F(ab′)$_2$ fragment donkey anti-rabbit IgG (# 711-036-152; 1:500) were purchased from Jackson ImmunoResearch. Inhibitors used were: LY 294002 from Cayman Chemicals and class-I-specific PIK-75 and BYL719 from Selleck Chemicals. Membrane lipid strips and PI(4,5)P_2 Grip (PLC-δ1-PH) were purchased from Echelon. 3-Amino-1,2,4-triazole (ATA), Triton X-100 (TX-100), paraformaldehyde (PFA), adenosine 5′-triphosphate disodium salt hydrate (ATP), guanosine 5′-triphosphate sodium salt hydrate (GTP), phosphocreatine disodium salt hydrate (CP), phosphocreatine kinase (CPK), poly-L-lysine solution, saponin and fatty-acid-free bovine serum albumin (FAF-BSA) were from Sigma-Aldrich. Poly-L-lysine-coated coverslips were from BD Biosciences. PD-10 dye removal columns and PD MiniTrap G-25 were purchased from GE Healthcare Life Sciences. inositol 1,3,4,5-tetrakisphosphate (IP_4) was purchased from Cell Signals. All other materials (salts and organic solvents) were of analytical grade.

Recombinant protein purification and specificity testing

E. coli cells were transformed with pGEX plasmid containing GST–Grp1-PH. A resulting colony was used to inoculate a Luria broth (LB) culture, which was grown at 37°C, with shaking at 200 rpm. Protein expression was induced at OD_{600} 0.6 with 1 mM IPTG at 18°C overnight. Cells were harvested by centrifugation at 11,000 ***g*** for 20 min at 4°C, resuspended in distilled water and treated with 10 mg of lysozyme. The suspensions were frozen overnight at −20°C and, the following day, resuspended in 10× lysis buffer [500 mM Tris-HCl, pH 7.4, 10% (v/v) Triton X-100, 20 mM EDTA, 10 mM DTT, 10 mM AEBSF] before probe sonication for 5 min. After centrifugation at 12,000 ***g*** for 20 min at 4°C to remove cell debris, the supernatant was loaded onto 0.5 ml of slurry of glutathione Sepharose beads that had been pre-equilibrated in 50 mM Tris-HCl, pH 7.4, 140 mM NaCl, 2.7 mM KCl. The sample was incubated for 15 min at 4°C. Two washes with equilibration buffer (pre-equilibration buffer supplemented with 2 mM DTT) and two further washes with equilibration buffer supplemented with 500 mM NaCl were performed. Recombinant GST-tagged protein was eluted by adding 0.5 ml of elution buffer (50 mM Tris-HCl, pH 7.4, 20 mM glutathione, 250 mM NaCl, 2 mM DTT, 20% glycerol), vortexing and incubating for 10 min on ice. Aliquots of the eluted fractions were analysed by SDS-PAGE on a 4–12% NuPAGE pre-cast gel (Invitrogen). The eluted protein was quantified by Bradford assay. To corroborate that the purified

Journal of Cell Science (2017) 130, 444-452 doi:10.1242/jcs.193771

protein was the protein of interest, a western blot was performed with an anti-GST antibody.

The construct was also identified by protein mass spectrometry. For this, it was first detected by Coomassie Blue staining, and the band of the expected molecular mass (44 kDa) was excised, diced and sent for analysis (in collaboration with the Protein Analysis Facility, Clare Hall, Cancer Research UK). Excised protein bands were subjected to in-gel trypsin digestion using a Perkin-Elmer Janus Automated Workstation. Peptide mixtures were acidified to contain 0.1% formic acid and injected onto a nanoACQUITY UPLC instrument (Waters Corporation) coupled to an LTQ-Orbitrap XL (Thermo Fisher Scientific) through an Advion Biosciences Nanomate. Peptides were eluted over a 30 min gradient [5–40% (v/v) acetonitrile]. Peak lists were extracted using Mascot distiller and searched with Mascot v.2.4.1 (Matrix Science) against the UniProt reference database. Oxidation of methionine was entered as a variable modification and the search tolerances were 5 ppm and 0.8 Da for peptides and fragments, respectively. Searches were compiled in Scaffold 4.1.1.

GST–Grp1-PH probe specificity was demonstrated using dot blots, as described previously (Jethwa et al., 2015). Commercial lipid strips were incubated with blocking buffer (3% FAF-BSA, 0.1% Tween-20 PBS) for 1 h at room temperature. 1 µg/ml of GST–Grp1-PH in blocking buffer was added and incubated for 1 h at room temperature. Excess buffer was washed with PBS-T (five washes, 5 min each). Then, anti-GST antibody (1:2500) was added in blocking buffer, incubated for 1 h at room temperature and washed as before. Finally, anti-mouse HRP-conjugated antibody (1:5000) in blocking buffer was added and incubated for 1 h at room temperature. Washes were performed as above and rinsed with PBS. Blots were photo-activated with a 1:1 mixture of the Amersham ECL reagents and exposed to photographic AGFA Cronex 5 Medical X-Ray Film in a Kodak BioMax MS cassette for various periods of time. The films were developed using the IGP Compact2 Developer.

Nuclei and egg extracts

Gamete shedding and collection of *P. lividus* took place as described previously (Byrne et al., 2009b) through intracoelomic injection of 0.5 M KCl. Sea urchin sperm was permeabilised with 0.1% Triton X-100, and fertilised egg cytoplasmic extract (S10) was prepared by twice vigorously homogenising the egg suspension 10 min after fertilisation with a syringe with a 22-gauge, 1.5-inch needle and centrifugation to remove the yolk (upper layer) and the pigment pellet (Byrne et al., 2009b). The S10 fraction, which includes cytosol and cytoplasmic membrane vesicles, can be subsequently fractionated using a sucrose gradient to separate the different membrane vesicle populations (MV1, MV2, etc.) that contribute to nuclear envelope formation (Byrne et al., 2009b).

Cell-free assembly of the male pronucleus

De-membraned sperm nuclei were mixed with the S10 fraction and an ATP-generating system (1:1:1 ATP:creatine phosphate:creatine phosphate kinase ratio) and incubated for 1 h at room temperature. Nuclei were decondensed, and membrane vesicles were bound to chromatin after this time. Then, GTP (1 or 5 mM final concentration) was added and incubated for 2 h at room temperature to initiate nuclear envelope formation. The reaction was stopped by diluting the samples approximately sevenfold with cold lysis buffer (10 mM Hepes, pH 8.0, 250 mM NaCl, 5 mM $MgCl_2$, 110 mM glycine, 250 mM glycerol, 1 mM DTT, 1 mM AEBSF). For analysis, samples were settled in poly-L-lysine-coated coverslips and fixed with 3.7% PFA in isolation buffer.

For inhibitor studies of nuclear envelope assembly, LY 294002, PIK-75 or BYL719 were added before the GTP addition and incubated for 15 min.

Sea urchin egg time series

Eggs were collected in Millipore-filtered sea water (MPSW) and dejellied by passing them twice through a Nytex mesh of the appropriate pore size (210 µm) (Foltz et al., 2004). Subsequently, the eggs were fertilised and left on a rotator shaker. At various time points, post-fertilisation eggs were fixed by mixing 1 ml of the egg suspension with 1 ml of 7.4% PFA in cold isolation buffer (80 mM Pipes, pH 7.2, 5 mM EGTA, 5 mM $MgCl_2$, 1 M glycerol). Fixation was terminated after 1 h of gentle shaking. The eggs were centrifuged (150 ***g***, 4°C, 1 min) and washed twice with PBS. Finally, eggs were resuspended in 0.05% azide in PBS and stored at 4°C.

For inhibitor studies, inhibitors were added to eggs 3–4 min after fertilisation. Aliquots were fixed and stored as described above.

Immunofluorescence

For confocal imaging of the cell-free assay, nuclei were labelled by adding Hoechst 33342 (2 µg/ml), and membranes were labelled with $DiOC_6$ (2 µM), both in TBS. If GST–Grp1-PH was added, the sample was blocked with 3% FAF-BSA in TBS for 15 min before the recombinant protein was added in 3% FAF-BSA in TBS, and incubated for 1 h. The excess was washed with TBS, followed by labelling with Dylight650-conjugated anti-GST antibody (1:500) for 1 h. Secondary antibody alone was incubated as a control with nuclei to check the absence of signal.

Intact eggs were blocked and permeabilised before antibody addition by incubating the cells with 3% FAF-BSA and 0.5–1% saponin in TBS for 15–50 min. Then, the required antibodies were introduced into the buffer (3% FAF-BSA 0.5% saponin TBS), and samples were incubated for 1 h on an overhead mixer and washed after each incubation.

After labelling and settling onto poly-L-lysine-coated coverslips, ProLong reagent was used to mount slides. Image acquisition was performed on a Zeiss 710 upright confocal microscope run by Zen software (2009), with a 63×1.4NA oil immersion objective and the custom filter set-up for the probes as indicated; or an inverted confocal fluorescence microscope Nikon D-ECLIPSE C1 (Nikon Inc., Melville, N.Y.) with a 60×1.4 NA oil immersion objective.

Inhibitors used in the cell-free assay

In the cell-free experiments, when inhibitors were added, the formation of the nuclear envelope of at least 100 nuclei was scored in three independent experiments using a wide-field inverted Eclipse-Ti microscope (Nikon) PL APO 60×1.4 NA oil immersion objective. Because inhibitors were added in DMSO, the corresponding vehicle controls were performed.

Quantification of colocalisation

The threshold for every image was subjected to the algorithm moments (ImageJ software). This method keeps the moments of the original image in each thresholded result (Tsai, 1985).

The regions of interest were selected, and the colocalisation was calculated in the following manner. The colocalisation of the various proteins and phospholipids under investigation were analysed only in a region of interest around the female pronucleus, in unfertilised eggs, or in female and male pronuclei in fertilised eggs. This was performed in order to mainly focus on processes occurring within the vicinity of the nuclear envelope. The colocalisation measured in these regions of interest was expressed as a percentage of the total number of pixels in each region of interest – i.e. the ratio of pixels in two different channels (corresponding to the two fluorescent labels) relative to the total number of pixels in the regions of interest. These were plotted as box and whisker plots, and the statistics were performed using a non-parametric Mann–Whitney test. This quantification was performed for at least ten eggs for each condition.

Data acquisition for the measurement of FRET

Fixed eggs were blocked and permeabilised as described above. Cell autofluorescence was quenched with 2 mg/ml of sodium borohydrate ($NaBH_4$) in PBS for 2 min, and endogenous peroxidase activity was suppressed by incubating the cells with the specific reagent for 20 min. Proteins were labelled with anti-Rab7 antibody followed by anti-chicken F(ab′)$_2$–Atto-488, and lipids were labelled with GST–Grp1-PH and then an anti-GST antibody followed by anti-rabbit F(ab′)$_2$ conjugated to HRP. All antibody incubations took place in 3% FAF-BSA with 0.5% saponin in PBS for 1 h. To create an enhanced acceptor signal, eggs were treated with TSA–Alexa-Fluor-594 for 10 min at room temperature (Byrne et al., 2014; Veeriah et al., 2014), as per the manufacturer's instructions, with the enhancement reaction being terminated by PBS washes (150 ***g***, 1 min). Eggs were additionally labelled with 2 µg/ml Hoechst 33342 and mounted in ProLong Gold.

A multiple frequency domain FLIM lifetime imaging microscope from Lambert Instruments was used, and samples were excited with the 473-nm diode laser. Images were acquired on an Eclipse-Ti microscope (Nikon) PL APO 60×1.4 NA oil-immersion objective. FRET efficiency (E_f) was determined using the following formula: $E_{f\ (\%)}=[1-(t_{DA}/t_D)]\times100$; where t_D is donor lifetime and t_{DA} is the donor plus acceptor lifetime. Only samples with donor intensity at least two times higher than the autofluorescence intensity were included for FRET efficiency calculations.

Conjugation of Atto-488 to anti-chicken F(ab′)$_2$ fragments

100 µg of anti-chicken F(ab′)$_2$ antibody was conjugated to 25 µg of chromophore in a 100-µl volume adjusted to pH 8.5 with 50 mM sodium borate buffer. Atto-488 (donor chromophore) was conjugated to an anti-chick F(ab′)$_2$ fragment for 1 h in the dark at 20°C with shaking. Free chromophore was separated from antibody–dye conjugate on a PD Minitrap™ G-25 column (GE Healthcare). The dye-to-protein ratio of the chromophore–antibody conjugate was calculated as per the manufacturer's instructions. Conjugates had a dye-to-protein ratio of <3:1.

Statistical analyses

Statistical analysis for the box and whisker plots was performed using the Origin software. Boxes represent the 25–75% percentiles of the data set, and the whiskers represent 100% of the population. Individual data points are shown as diamonds. Statistical significance between the groups was calculated with Mann–Whitney test. For other graphs, statistical analysis was performed in SigmaPlot subjecting data to an unpaired *t*-test. Differences were considered statistically significant when $P\leq0.05$.

Acknowledgements

We thank Gloria de Las Heras and Unai Lorenzo for their help with the image software analysis.

Competing interests

The authors declare no competing or financial interests.

Author contributions

M.G.L., R.D.B. and B.L. designed the experiments; M.G.L., D.L.P. and B.L. wrote the manuscript; M.G.L. performed the experiments; A.A. provided reagents and financial support; all authors reviewed and approved the manuscript prior to submission.

Funding

We also acknowledge the support of the Ikerbasque, Basque Foundation for Science to B.L.; the Ministerio de Economía y Competitividad to A.A. [MINECO-FEDER; BFU2015-66306-P (to A.A.) and BFU2015- 65625-P (to B.L.)]; Eusko Jaurlaritza (the Basque Government) [IT838-13] to B.L.; and a Faculty Research Award of the Axel Schupf '57 Fund for Intellectual Life and Senior Sabbatical Fellowship, Amherst College [448125] to D.P. M.G.L. was a doctorate fellow supported by Eusko Jaurlaritza.

Supplementary information

Supplementary information available online at
http://jcs.biologists.org/lookup/doi/10.1242/jcs.193771.supplemental

References

Burke, B. and Ellenberg, J. (2002). Remodelling the walls of the nucleus. *Nat. Rev. Mol. Cell Biol.* **3**, 487-497.

Byrne, R. D., Garnier-Lhomme, M., Han, K., Dowicki, M., Michael, N., Totty, N., Zhendre, V., Cho, A., Pettitt, T. R., Wakelam, M. J. et al. (2007). PLCgamma is enriched on poly-phosphoinositide-rich vesicles to control nuclear envelope assembly. *Cell. Signal.* **19**, 913-922.

Byrne, R. D., Poccia, D. L. and Larijani, B. (2009a). Role of phospholipase C in nuclear envelope assembly. *Clin. Lipidol.* **4**, 103-112.

Byrne, R. D., Zhendre, V., Larijani, B. and Poccia, D. L. (2009b). Nuclear envelope formation in vitro: a sea urchin egg cell-free system. *Methods Mol. Biol.* **464**, 207-223.

Byrne, R. D., Applebee, C., Poccia, D. L. and Larijani, B. (2012). Dynamics of PLCgamma and Src family kinase 1 interactions during nuclear envelope formation revealed by FRET-FLIM. *PLoS ONE* **7**, e40669.

Byrne, R. D., Veeriah, S., Applebee, C. J. and Larijani, B. (2014). Conservation of proteo-lipid nuclear membrane fusion machinery during early embryogenesis. *Nucleus* **5**, 441-448.

Collas, P. and Poccia, D. (1996a). Distinct egg membrane vesicles differing in binding and fusion properties contribute to sea urchin male pronuclear envelopes formed in vitro. *J. Cell Sci.* **109**, 1275-1283.

Collas, P. and Poccia, D. L. (1996b). Conserved binding recognition elements of sperm chromatin, sperm lipophilic structures and nuclear envelope precursor vesicles. *Eur. J. Cell Biol.* **71**, 22-32.

Collas, P. and Poccia, D. (1998). Remodeling the sperm nucleus into a male pronucleus at fertilization. *Theriogenology* **49**, 67-81.

Domart, M.-C., Hobday, T. M. C., Peddie, C. J., Chung, G. H. C., Wang, A., Yeh, K., Jethwa, N., Zhang, Q., Wakelam, M. J. O., Woscholski, R. et al. (2012). Acute manipulation of diacylglycerol reveals roles in nuclear envelope assembly & endoplasmic reticulum morphology. *PLoS ONE* **7**, e51150.

Dumas, F., Byrne, R. D., Vincent, B., Hobday, T. M. C., Poccia, D. L. and Larijani, B. (2010). Spatial regulation of membrane fusion controlled by modification of phosphoinositides. *PLoS ONE* **5**, e12208.

Ferguson, K. M., Kavran, J. M., Sankaran, V. G., Fournier, E., Isakoff, S. J., Skolnik, E. Y. and Lemmon, M. A. (2000). Structural basis for discrimination of 3-phosphoinositides by pleckstrin homology domains. *Mol. Cell* **6**, 373-384.

Foltz, K. R., Adams, N. L. and Runft, L. L. (2004). Echinoderm eggs and embryos: procurement and culture. *Methods Cell Biol.* **74**, 39-74.

Jethwa, N., Chung, G. H., Lete, M. G., Alonso, A., Byrne, R. D., Calleja, V. and Larijani, B. (2015). Endomembrane PtdIns(3,4,5)P3 activates the PI3K/Akt pathway. *J. Cell Sci.* **128**, 3456-3465.

Klarlund, J. K., Tsiaras, W., Holik, J. J., Chawla, A. and Czech, M. P. (2000). Distinct polyphosphoinositide binding selectivities for pleckstrin homology domains of GRP1-like proteins based on diglycine versus triglycine motifs. *J. Biol. Chem.* **275**, 32816-32821.

Larijani, B., Barona, T. M. and Poccia, D. L. (2001). Role for phosphatidylinositol in nuclear envelope formation. *Biochem. J.* **356**, 495-501.

Olmos, Y., Hodgson, L., Mantell, J., Verkade, P. and Carlton, J. G. (2015). ESCRT-III controls nuclear envelope reformation. *Nature* **522**, 236-239.

Poccia, D. and Larijani, B. (2009). Phosphatidylinositol metabolism and membrane fusion. *Biochem. J.* **418**, 233-246.

Prunuske, A. J. and Ullman, K. S. (2006). The nuclear envelope: form and reformation. *Curr. Opin. Cell Biol.* **18**, 108-116.

Raiborg, C., Wenzel, E. M., Pedersen, N. M., Olsvik, H., Schink, K. O., Schultz, S. W., Vietri, M., Nisi, V., Bucci, C., Brech, A. et al. (2015). Repeated ER-endosome contacts promote endosome translocation and neurite outgrowth. *Nature* **520**, 234-238.

Sato, I., Obata, Y., Kasahara, K., Nakayama, Y., Fukumoto, Y., Yamasaki, T., Yokoyama, K. K., Saito, T. and Yamaguchi, N. (2009). Differential trafficking of Src, Lyn, Yes and Fyn is specified by the state of palmitoylation in the SH4 domain. *J. Cell Sci.* **122**, 965-975.

Shinde, S. R. and Maddika, S. (2016). PTEN modulates EGFR late endocytic trafficking and degradation by dephosphorylating Rab7. *Nat. Commun.* **7**, 10689.

Stenmark, H. (2009). Rab GTPases as coordinators of vesicle traffic. *Nat. Rev. Mol. Cell Biol.* **10**, 513-525.

Tsai, W.-H. (1985). Moment-preserving thresolding: A new approach. *Comput. Vision Graphic. Image Process.* **29**, 377-393.

Tu, C., Ahmad, G., Mohapatra, B., Bhattacharyya, S., Ortega-Cava, C. F., Chung, B. M., Wagner, K.-U., Raja, S. M., Naramura, M., Band, V. et al. (2011). ESCRT proteins: Double-edged regulators of cellular signaling. *Bioarchitecture* **1**, 45-48.

Veeriah, S., Leboucher, P., de Naurois, J., Jethwa, N., Nye, E., Bunting, T., Stone, R., Stamp, G., Calleja, V., Jeffrey, S. S. et al. (2014). High-throughput time-resolved FRET reveals Akt/PKB activation as a poor prognostic marker in breast cancer. *Cancer Res.* **74**, 4983-4995.

Vietri, M., Schink, K. O., Campsteijn, C., Wegner, C. S., Schultz, S. W., Christ, L., Thoresen, S. B., Brech, A., Raiborg, C. and Stenmark, H. (2015). Spastin and ESCRT-III coordinate mitotic spindle disassembly and nuclear envelope sealing. *Nature* **522**, 231-235.

Journal of Cell Science